Myeloid-secreted BDNF maintains innervation of inguinal adipose in male mice

Magdalena Blaszkiewicz[1,2], Elizabeth Wood[1], Sigi Koizar[1], Jake W. Willows[1], Lei Cao[3], Wei Huang[3], James Godwin[4,5], Kristy L. Townsend*[1,2]

[1]School of Biology and Ecology, University of Maine, Orono, ME
[2]Graduate School of Biomedical Science and Engineering, University of Maine, Orono, ME
[3]The Ohio State University, Columbus OH
[4] Jackson Laboratory, Bar Harbor ME
[5]MDI Biological laboratory, Bar Harbor ME

*Corresponding Author

kristy.townsend@maine.edu; 207-581-2541
5735 Hitchner Hall, Rm 301, Orono ME 04469

Running Title: Myeloid-secreted BDNF maintains adipose innervation

Key Words: Innervation, white adipose tissue (WAT), energy expenditure, browning, CINCs, cold-induced neuroimmune cells

Graphical Abstract

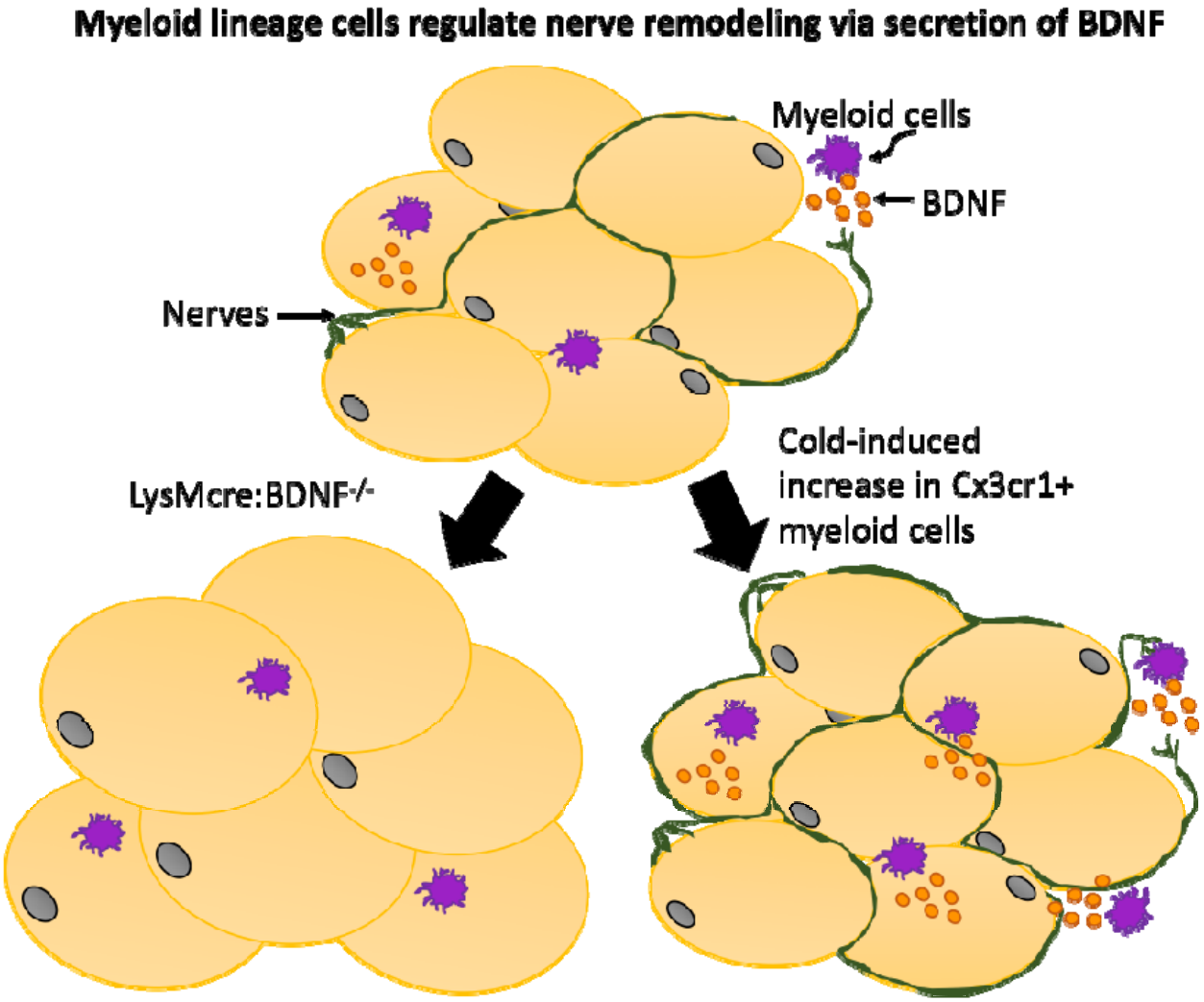

Abstract

Innervation of adipose tissue is essential for the proper function of this critical metabolic organ. Numerous surgical and chemical denervation studies have demonstrated how maintenance of brain-adipose communication through both sympathetic efferent and sensory afferent nerves helps regulate adipocyte size, cell number, lipolysis, and 'browning' of white adipose tissue. Neurotrophic factors are growth factors that promote neuron survival, regeneration and outgrowth of neurites from adult nerves. Peripheral blood immune cells have been shown to be a source of neurotrophic factors in humans and mice. Although a number of these immune cells also reside in the adipose stromal vascular fraction (SVF), it has remained unclear what roles they play in adipose innervation. We have demonstrated that adipose resident myeloid lineage immune cells secrete brain derived neurotrophic factor (BDNF) and that deletion of this neurotrophic factor from the myeloid lineage led to a 'genetic denervation' of inguinal subcutaneous adipose tissue, thereby causing decreased energy expenditure and increased adipose mass. AAV-BDNF intra-adipose injections resulted in an increase in markers of innervation in two models with demonstrated adipose neuropathy. We and others have previously shown that noradrenergic stimulation via cold exposure increases adipose innervation in the inguinal depot. Here we have identified a subset of myeloid cells that are Cx3cr1+ monocytes/macrophages expressing adrenergic receptors. The quantity of these mobile immune cells increased in adipose tissue upon cold stimulation, fitting with their function to hone to sites of tissue injury and repair, and these cells also expressed BDNF. We propose that these cold induced neuroimmune cells (CINCs) are key players in maintaining adipose innervation as well as promoting adipose nerve remodeling under adrenergic stimuli such as cold exposure.

Introduction

In order for the central nervous system (CNS) to regulate functions of distal organs, peripheral innervation of tissues needs to be maintained and properly coordinated. It has been demonstrated numerous times that loss of innervation of the adipose organ (by surgical or chemical means) leads to dysfunction of the tissue and disrupts whole body energy homeostasis. Denervation of brown adipose tissue (BAT) greatly impairs the energy expending process of adaptive thermogenesis [1-4], while denervation of white adipose tissue (WAT) results in fat mass accumulation via hyperplasia and impaired lipolysis [5-7]. Furthermore, we have demonstrated that nerves in subcutaneous adipose tissue (scWAT) undergo remodeling in response to pathophysiological and environment stimuli, and exhibit signs of neuropathy in obesity/diabetes as well as with aging [8]. Cold exposure served to enhance neurite density within the scWAT depot [8].

Nerve remodeling is facilitated by neurotrophic factors (NFs) both in the CNS [9] and in peripheral nerves [10]. NFs are nerve growth factors that support nerve health, survival, and plasticity. Brain derived neurotrophic factor (BDNF) is one member of the neurotrophin family of NFs, which in mammals also includes nerve growth factor (NGF), Neurotrophin-3 (NT-3), and Neurotrophin-4/5 (NT-4/5). Neurotrophins signal predominantly through Trk receptors on nerves, through which they are endocytosed and, in peripheral nerves, transported in a retrograde manner to the nerve cell body. BDNF has been well studied for its role in hippocampal synaptic plasticity in the adult brain [11-13], as well as learning and exercise related neurogenesis [14]. BDNF is also an important modulator of energy balance through its actions in the hypothalamus [14]. Deletion of *Bdnf* in the ventromedial and dorsomedial regions of the hypothalamus

resulted in an obesity phenotype due to hyperphagic behavior [15]. Obesity is associated with lower serum levels of BDNF in humans, and animal studies have shown that central and peripheral administration of BDNF reduced food intake and hyperglycemia, and increased energy expenditure, via CNS mediated mechanisms [16-18]. As review by Xu and Xie, genetic mutations in human BDNF and its receptor TrkB result in morbid early-onset obesity [19]; furthermore, genome wide associated studies (GWAS) have identified single nucleotide polymorphisms (SNPs) in or near *BDNF* to be associated with increased BMI [19].

Despite these strong correlations between altered function of BDNF and its receptor TrkB with obesity, this growth factor has been predominately studied only in the CNS. A few studies have clearly shown that NFs, including BDNF, are present in adipose tissue [20-22], but the cellular source of BDNF in adipose had not been determined. In adipose specific (*FABP4-Cre*) knock-outs of BDNF or TrkB, only CNS effects were apparent (not surprising given off-target brain effects of this cre line). Using instead an *adipoq*-cre (mature adipocyte-specific line) there was no obesity in a BDNF or a TrkB KO, and the BDNF KO showed no difference in adipose BDNF levels, suggesting that mature adipocytes are *not* the cellular source of BDNF [23], which we have confirmed in this study. NFs are secreted by glial cells in the brain [24] and Schwann cells in peripheral tissues [25]. However, other cell types, predominantly immune cells, are also known sources of NFs [26-30].

As part of the immune response to injury, immune cells are critical players in wound healing, regeneration, and remodeling of various tissues. They are an important component of the adipose organ where they modulate the inflammatory response, clear the tissue of apoptotic cells, and mediate adipose tissue remodeling during obesity

through an influx of monocytes (undifferentiated macrophages), neutrophils, T cells, B cells and mast cells [31-36]. Macrophages and their monocyte precursors are myeloid lineage immune cells and comprise the highest fraction of immune cells present in adipose tissue [37]. They are highly heterogeneous cells that are polarized by environmental stimuli to evoke differential responses within a tissue, including secretion of cytokines.

In a simplistic paradigm, classically activated macrophages (M1) act in a pro-inflammatory manner, while alternatively activated macrophages (M2) produce an anti-inflammatory response and initiate tissue remodeling after injury. Both M1 and M2 cells retain phagocytic behavior. During obesity, M1 adipose tissue macrophages (ATMs) greatly increase in number, thus contributing to a chronic state of tissue inflammation [38]; and inflamed, insulin-resistant adipose tissue histology is characterized by macrophage crown-like structures surrounding hypertrophic, hypoxic and dying adipocytes. On the other hand, it has been suggested that cold-induced browning of adipose promotes an M2 phenotype in ATMs [38], possibly promoting tissue remodeling and potentially serving as a source of NFs in adipose tissue. Importantly, the immunology field has uncovered that M1 and M2 designations are an oversimplification, where many immune cells express markers of both subtypes and may be inter-converting between the two polarities, but this has never been clearly demonstrated in adipose tissues.

Although myeloid cells, including monocytes and macrophages, from peripheral blood have been shown to store and release NFs [39], it is still unclear what role these immune cells play in peripheral innervation, and it remains unknown how and if adipose-resident immune cells are stimulated to release NFs that act locally. Microglia, or the

CNS resident myeloid cells that are most similar to macrophages, are an accepted source of BDNF in the brain [40] and increase secretion of BDNF in response to neuroinflammation [41]. Microglial-derived BDNF in the CNS promotes hippocampal synaptic plasticity [40] and neurogenesis [42]. We hypothesized that myeloid lineage cells may play a similar role in adipose tissue, and generated a myeloid specific BDNF knock-out mouse model, by crossing *LysM*$^{cre/-}$ and *BDNF*$^{fl/fl}$ mice. Here we report a role for myeloid derived BDNF in the specific maintenance of adipose innervation, and identify a subpopulation of monocyte/macrophages (Cx3cr1+) that infiltrate adipose tissue in response to cold stimulation and express BDNF.

Materials and Methods

Mice, Metabolic Phenotyping, and in vivo Analyses

Animals

The following mouse strains were obtained from The Jackson Laboratory: C57BL/6J (Stock # 000664); LysM$^{cre/-}$ (B6.129P2-Lyz2/J, Stock # 004781); BDNF$^{fl/fl}$ (Bdnf^{tm3Jae}/J, Stock # 004339); R26R-EYFP (B6.129X1-Gt(ROSA)26Sortm1(EYFP)Cos/J, Stock # 006148. Animals with myeloid specific deletion of BDNF (LysM^{cre}:BDNF$^{-/-}$) were generated in our facility by crossing mice heterozygous for the myeloid -specific cre transgene (LysM^{cre}) with mice homozygous for floxed BDNF. Reporter mice were generated by crossing LysM^{cre}x BDNF^{flfl} x R26R-EYFP. Male C57BL/6J mice (Jackson Laboratory, Bar Harbor, ME; stock number 000664 Black 6) and BTBR $^{ob/ob}$ mutant (MUT) mice (Jackson Laboratory, Bar Harbor, ME; BTBR.Cg-Lepob/WiscJ, stock number 004824) were used for AAV-BDNF gene delivery studies. Animals were housed 3-5 to a cage providing for socialization, in a monitored temperature and humidity-

controlled environment with 12/12hr light/dark cycle. Cages were replaced weekly, ad libitum access to food and water was maintained. For all studies animals were sacrificed using CO_2 followed by cervical dislocation.

Dietary fat interventions and food intake

Adult male *LysM*^{cre}*:BDNF*$^{-/-}$ mice were a 45% HFD diet from Research Diets (New Brunswick, NJ) for up to 11 weeks. Mice were housed 2-3 per cage, at room temperature. Body weight was measured weekly. Food intake was measured daily for 7 days, then weekly until the end of the experiment. Adiposity was assessed at the end of the study by weighing intact adipose depots after surgical removal.

CLAMS

Metabolic cage analyses were conducted in a Comprehensive Laboratory Animal Monitoring System (CLAMS; Columbus Instruments, Columbus, OH), for measurement of oxygen consumption (VO_2) and carbon dioxide production (VCO_2), from which both respiratory exchange ratio (RER), and energy expenditure (heat) were calculated: *RER=*VCO_2/VO_2; *Energy expenditure (heat) = CV * VO_2 cal/hr, where CV is the "caloric value" as given by CV = (3.815 + 1.232) * RER.* Animal were single housed in a bedding free cage, at room temperature on a 12hr light/dark cycle. Mice were acclimated for 24-48hrs, after which VO_2, VCO_2, RER, and Heat were measured every 15min for 3 days (72hrs). Waveform analysis of CLAMS data was performed by matching every 15min measurement across all three 24hr-cycles. Two-way repeated measures analysis of variance (RM, ANOVA) was performed for average VO_2, VCO_2, RER, and Heat per group. An uncorrected Fisher's Least Significance Difference test was performed for each time point between dietary groups as a post-hoc test. Interaction P values are

reported, which represent differences in 24hr data between groups, as well as multiple comparison results for differences which were only day/night phase specific.

CL Injections

Adult (12-13 week old) male C57BL/6 mice received daily i.p. injections of ADRβ3 agonist CL316,243 (Tocris Bioscience, Bristol, U.K.; Cat # 1499), at 1.0 mg/kg BW or an equivalent amount of sterile saline, for 10-14 days.

Cold Exposure Experiments

All cold exposure was carried out in a diurnal incubator (Caron, Marietta, OH, USA) at 5°C, and a 12hr light/dark cycle. Animals were housed two to a cage and continuously cold exposed for 3 - 14 days.

Glucose Tolerance Test (GTT)

Animals were fasted overnight for 16hr, after which they received an intraperitoneal (i.p.) bolus injection of 1g/kg glucose. Blood glucose was measured using tail vein blood with a hand-held glucometer (OneTouch UltraMini, LifeScan, Milpitas, CA, Johnson&Johnson, New Brunswick, NJ), at time 0 and at intervals of 15 minutes, 30 minutes, and 60 minutes after injection.

Western Blot

Protein lysates were prepared by homogenizing frozen whole adipose depots in RIPA buffer using a Bullet Blender (Next Advance, Averill Park, NY), followed by Bradford Assay, and preparation of equal-concentration lysates in Laemmli buffer. 60ug of protein was loaded per lane of a 10% polyacrylamide gel, and following gel running, proteins were transferred to PVDF membranes for antibody incubation. Primary antibodies used included: anti-PGP9.5 (Abcam, Cambridge, U.K. Cat. #10404 and

#108986) used at a 1:1000 and 1:500 dilutions respectively; anti-UCP1 (Abcam, Cambridge, U.K. Cat. #10983) used at 1:1000 dilution, anti-TH (Millipore Cat. # AB152; Merck Millipore, Burlington, MA), anti-β-tubulin (Cell Signaling Technology, Danvers, MA, USA; Cat. # 2146BC), were all used at 1:1000 dilution. Secondary antibody was anti-rabbit HRP (Cell Signaling Ct # 7074), used at a 1:3000 dilution. Blots were visualized with enhanced chemiluminescence (ECL; Pierce) on a Syngene G:BOX. Protein expression of PGP9.5, TH, and UCP1 was normalized to either -β-tubulin or β-actin and quantified in Image J.

Collection of adipose secretions and BDNF ELISA

BAT depots were dissected, weighed and minced in a petri dish containing DMEM (high-glucose, serum-free). Minced tissue was transferred to a 15mL conical tube, with 5mL DMEM (loosely capped to keep tissue oxygenated) and placed in a shaking water bath at 37°C. Secretions were collected at time 0, 1hr, 2hrs, and 3hrs (1mL collected from conical tube at each time point and replaced with 1mL fresh DMEM). Secretions were stored at -80°C until processing. For ELISA, protein secretions were concentrated using Amicon ® Ultra Centrifugal Filters, Ultracel ® -100K (Millipore, Burlington, MA USA; Cat. # UFC510096), per manufacturer's instructions. Mouse BDNF PicoKine™ ELISA Kit (Boster Biological Technology, Pleasanton, CA, USA; Cat# EK0309) was used per manufacturer's instruction to determine amount of BDNF present in adipose active secretions.

Thyroid hormone ELISA

Mouse sera were used to measure circulating levels of thyroxine (T4) and triiodothyronine (T3). Circulating concentrations were determined by Enzyme-Linked Immunosorbant Assays (ELISA) at Maine Medical Center Research Institute's Core Facilities (Scarborough, ME).

SVF isolation

Bilateral whole inguinal adipose depots were quickly dissected and weighed. Tissue was minced in 37°C pre-warmed DMEM (high glucose, serum free) containing 2mg/mL Roche Collagenase A (Millipore-Sigma, St. Louis, MO; Cat# 10103586001) at a volume of 10mL/depot. Minced tissue with collagenase containing DMEM was placed in a 50mL conical tube and transferred to a shaking water bath (350/min rotation) at 37°C. Every 10min cells were dispersed by vortex and pipette mixing. Full dissociation was usually achieved within 2hrs, when adipocytes were clearly visible and all tissue was dissociated. Dissociated media was poured through 100um cell strainers, rinsed with DMEM and centrifuged at 500g for 10min to separate adipocytes from SVF. After centrifugation adipocytes were collected (found floating on top); remainder of DMEM was removed sparing the SVF pellet. SVF pellet was incubated with 500uL of RBC lysis buffer on ice for 2min, after which 2mL od DMEM with serum was added to stop lysis. Cells were centrifuged at 500g for 5min at 4°C, and either collected for RNA or resuspended in FACS/MACS buffer for cell sorting.

Magnetic-activated Cell Sorting (MACS)

SVF from bilateral whole inguinal adipose depots was isolated as described above and resuspended in degassed buffer (1XPBS pH7.2, 0.5% BSA and 2mM EDTA). Single-

cell suspensions were sorted on the MidiMACS Quadro magnetic-activated cell separator system (Miltenyi Biotec, Bergisch Gladbach, Germany) according to manufactures instructions. Briefly, cells were stained with primary PE-conjugated antibody, CD11b-PE (Cat #130-098-087); a 1:10 antibody dilution per 10^7 cells was used. Cells were incubated for 10min at 4-8°C, washed, and centrifuged at 300g for 10min. Washed cell pellet was resuspended in a 1:10 dilution of anti-PE microbeads included in Anti-PE MultiSort Kit (Cat. #130-090-757). Following 15min incubation at 4-8°C, cells were washed and centrifuged as dercribed above. Cells were resuspending in 500µL of buffer and passed through LS columns of the MACS separator. LS colums were prepped according to manufacturer's suggestion. Cells were washed 3 times, collected cells (CD11b-) were collected. LS colums were removed from the MACS separator and flushed with 5mL of buffer to release the magnetically labeled cell fraction (CD11b+). MicroBeads were removed using MicroSort release reagent included in Anti-PE MultiSort Kit (Cat. #130-090-757). MicroBead free CD11b+ cell fraction was labeled for the secondary marker, Anti-F4/80-APC (Cat. #130-102-942), following the same procedure as described for the primary marker, except that Anti-APC MicroBeads (Cat. #130-090-855) were used.

20 cell surface marker tSNE Analysis of Myeloid Diversity in Male and Female Mice

Adult (13-15 week old) male and female control mice ($BDNF^{fl/fl}$) were cold exposed for 10 days in a diurnal incubator as described above. Following cold exposed SVF from bilateral whole inguinal adipose depots was isolated as described above. Single cell suspensions were treated with unlabeled FC receptor blocking antibody cocktail (CD16/CD32) in 50ul of FACS buffer (HBSS + 5mM EDTA + 2% FCS). Cells were then

incubated in an “staining antibody cocktail” against 20 cell surface markers for 60min at 4°C in 100ul. Cells were then washed in 1ml of FACS buffer and centrifuged at 400g for 7min, 2 times. Cells were then resuspended and analyzed on a five-laser 30-parameter FACSymphony A5 cytometer (BD Biocsiences, San Jose, USA) using DAPI exclusion for cell viability. For compensation of fluorescence spectral overlap, UltraComp eBeads (eBioscience, Inc.) were used following the manufacturer’s protocols. FCS 3.0 files generated by flow cytometry were initially processed using FlowJo Software (Tree Star, Ashland, USA) for automated compensation. Standard manual hierarchical gating was performed to remove debris, cell doublets, (DAPI+) dead cells from analysis before gating on CD45+ leukocyte populations. In preparation for performing the 20 marker tSNE leukocyte population analysis, the CD45+ population from each sample was down-sampled to 3000 events to normalize cellular input between samples. Using FlowJo, a concatemer of all samples was performed. An unbiased T-Distributed Stochastic Neighbor Embedding (tSNE) plugin algorithm was then run using defaults with 22 parameters, on the whole sample pool to obtain a multi-sample population reference map. Gating of each sample and experimental group was performed to generate tSNE maps for each condition. Differential cell clusters were gated and 20 marker histograms plots were used to predict cluster identities.

Antibodies used for adipose flow cytometric panel shown here: Anti-Mouse CD45-BUV395 (30-F11), Anti-Mouse B220_BUV496 (RA3-6B2), Anti-Mouse Ly-6G BUV563 (Clone 1A8), Anti-Mouse CD19 BUV661 (Clone 1D3), Anti-Mouse CD11b BUV737 (M1/70), Anti-Mouse NKp46_BV421 (29A1.4), Anti-Mouse CD62L BV510 (MEL-14), Anti-Mouse Ly6C_BV570 (HK1.4), Anti-Mouse CD3 BV605 (17A2), Anti-Mouse Mrc1_BV650 (C068C2), Anti-Mouse MHCII -I-A/I-E -BV711 (M5/114.15.2), Anti-Mouse

NK1.1 BV785 (PK136), Anti-Mouse CD11c_FITC (HL3), Anti-Mouse CD80 PE (16-10A1), Anti-Mouse CD115 CF594 (AFS98), Anti-Mouse Cx3CR1 PercP5.5 (SA011F11), Anti-Mouse CD64 PE-Cy7 (X54-5/7.1), Anti-Mouse CD14 APC (Sa2-8), Anti-Mouse CCR2 A700 (475301), Anti-Mouse F480 APC/Cy7 (BM8).

Fluorescence-activated Cell Sorting (FACS)

SVF from bilateral whole inguinal adipose depots was isolated as described above. For cell sorting, the following 5 marker panel was used with DAPI exclusion for viability: Anti-Mouse Ly6C_BV570 (HK1.4), Anti-Mouse CD11b PE (M1/70), Anti-Mouse Cx3CR1 PercP5.5, SA011F11), Anti-Mouse CD45-PE-Cy7 (30-F11), Anti-Mouse CCR2 A700 (475301). Sorting was performed on a BD™ FACSAria II™ cell sorter with SVF gated on CD45 and CD11b; CD45+CD11b- represented the non-myeloid population; CD45+CD11b+ myeloid fraction was gated on Ly6c, followed by CCR2 and Cx3cr1.

Gene Expression (qPCR)

RNA was isolated from whole tissue depots using Trizol reagent, and total RNA extracted using a Zymo (Irvine, CA) kit. RNA yield was determined on a Nanodrop; cDNA was synthesized using a High Capacity Synthesis Kit (Applied Biosystems, Foster City, CA). Real-time quantitative (q)PCR was performed with SYBR Green (Bio-Rad, Hercules, CA) on a CFX96 instrument (Bio-Rad, Hercules, CA).

Histology

Adipose

Immunofluorescent staining of 10% buffered formalin fixed, paraffin-embedded, 7uM sections of adipose tissues was performed for detection of UCP1 (1:500, Abcam, Cambridge, UK. Cat. #10983). Alexa 488 (2.5µg.mL, Molecular Probes, Eugene, OR, USA, Cat. # A11070) was used as secondary antibody. Typogen Black staining was used to quench tissue autofluorescence (prior to antibody incubation) and also provided visualization of cell size, browning (multilocularity) and crown-like structures. Stained sections were mounted using Millipore mounting fluid (Burlington, MA USA; Cat. # 5013) and 1 1/5 coverslips, and imaged on a Nikon Eclipse E400 epiflourescent microscope equipped with Nikon DS-fi2 camera.

Neuromuscular junction immunofluorescence, imaging, and analysis

Soleus and medial gastrocnemius muscles were removed and fixed in a 2% PFA at 4°C for 2 hours. Tissues were rinsed with 1XPBS and incubated in blocking buffer (1XPBS/2.5%BSA/0.5-1%Triton) at 4°C for at least 24 hours and up to 7 days. Following blocking muscles were teased, tendons and fat removed, and tissue was flattened by being placed between two tightly-bound glass slides for at least 30 minutes at 4°C. Tissues were transferred to fresh blocking buffer at 4°C for at least 12 hours. Immunostaining of innervation with primary antibodies was performed overnight at 4°C, followed by 1XPBS washes on a rotating platform at 4°C replacing PBS every 1hr for a total of 4-6hrs. Tissues were incubated with secondary fluorescent antibodies in similar fashion as primary antibodies. Primary antibodies included: neurofilament-M (2H3, 1:500) and synaptic vesicles (SV2, 1:250) from Developmental Studies Hybridoma Bank, (University of Iowa, USA). Secondary antibodies included: Alexa Fluor 488 at 1:500 (A21121) and alpha-bungarotoxin (BTX)-conjugated to Alexa Fluor 594 at 1:1000 (B13423) from Molecular Probes (Eugene, OR, USA). Tissues were mounted on

microscope slides using Millipore mounting fluid (Burlington, MA USA; Cat. # 5013) and 1 1/5 coverslips then sealed and allowed to set overnight. Stained sections were imaged on a Nikon Eclipse E400 epiflourescent microscope equipped with Nikon DS-fi2 camera. Brightness, contrast, and sharpness were adjusted in Microsoft PowerPoint. Up to 100 NMJs were counted for each tissue, statistics were conducted in GraphPad PRISM software (La Jolla, CA, USA) using the multiple t-tests (one-per row) function.

AAV Vector Construction and Package

HA-tagged human BDNF cDNA was subcloned into a novel AAV plasmid of dual cassettes that restricts off-target transduction in liver [43]. The rAAV plasmid contains a vector expression cassette consisting of the CMV enhancer and CBA promoter, WPRE, and bovine growth hormone (bGH) poly-A flanked by AAV2 inverted terminal repeats. Engineered hybrid serotype Rec2 vectors were packaged and purified as described previously [44].

AAV-BDNF delivery

Adult (16-week-old) male BTBR MUT mice were injected once in the left inguinal scWAT with $1x10^{10}$ vg of AAV-BDNF, while the right inguinal scWAT received an equal volume injection of vehicle (AAV buffer). Virus was constructed by Dr. Lei Cao as previously described [43]. Animals were carefully observed and scored for malaise for 48 hours after virus injection, and then observed daily, and showed no adverse reaction to the treatment. After 2 weeks animals were sacrificed, inguinal scWAT depots were harvested and processed for western blot analysis. In a separate study, adult (11-13 week old) male C57BL/6 mice were placed on a 58% HFD for 17 weeks to induce

neuropathy, as previously described [45]. At 17 weeks AAV-BDNF and vehicle were administered as described above. After 2 weeks animals were sacrificed, inguinal scWAT depots were harvested and processed for western blot analysis.

Statistical Analysis

For all animal experiments, mice were randomized to treatment groups to ensure no difference in starting body weight. All plots represent mean +/-SEM. Statistical calculations were carried out in Excel or GraphPad Prism software (La Jolla, CA, USA), utilizing ANOVA, Linear Regression, or Student's T-test as indications of significance (specified in Figure legends). Gene and protein expression data were normalized to a housekeeper and analyzed by either ANOVA or by Student's t-test, two-tailed, using Welch's correction when variance was unequal. Error bars are SEMs. For all figures, *$p < 0.05$, **$p < 0.01$, ***$p < 0.001$, ****$p < 0.0001$.

Ethical Statement

All procedures and handling of animals were performed in accordance with the University of Maine's Institutional Animal Care and Use Committee (IACUC), to comply with the guidelines of the PHS Policy on Humane Care and Use of Laboratory Animals, and Guide for the Care and Use of Laboratory Animals. This study was approved by the University of Maine's IACUC, under protocol A2017-09-04.

Results

BDNF is expressed primarily in adipose SVF

We previously demonstrated that BDNF levels increase in adipose tissue in response to noradrenergic stimulation, as administration of the β-3 adrenergic receptor (ADRβ3) agonist CL 316,243 resulted in an increase of BDNF secretion from the tissue [8]. We then endeavored to determine which adipose compartment and cell type was the source of local BDNF secretion in scWAT. Adipose tissue is a heterogeneous organ and although adipocytes are the main cell type, numerous other cell types are contained within the stromal vascular fraction (SVF) of adipose tissue. Adipose SVF consists predominantly of hematopoietic lineage cells including adipose tissue macrophages (ATMs [36, 37]), but also contains numerous other immune cell types, preadipocytes, vascular endothelial cells, and pericytes. To determine the compartmental source of adipose BDNF, adult male C57BL/6 mice were cold exposed and whole SVF was isolated from mature adipocytes of inguinal scWAT. Gene expression analysis revealed that *Bdnf* was almost exclusively expressed in the SVF, while other common NFs (nerve growth factor; NGF, and vascular endothelial growth factor, VEGFa) showed no difference of expression between SVF and mature adipocyte fractions (Fig. 1A). In FACS-sorted CD11b/F4/80 double-positive macrophages from scWAT SVF, BDNF was expressed and had no change with cold stimulation (Suppl. Fig. S1A). These data also indicated that non-F4/80 myeloid cells could express BDNF since those were contained in the negative sort that was also BDNF positive.

To determine the contribution of myeloid-lineage BDNF to adipose innervation, we created a knock-out (KO) mouse model using Cre-Lox technology. $LysM^{cre/-}$ mice were bred to $BDNF^{fl/fl}$ mice to generate $LysM^{cre/-}::BDNF^{fl/fl}$ (KO) animals, which lacked BDNF in myeloid lineage cells. Compared to littermate controls, KO animals exhibited a significant, although not complete, decrease of *Bdnf* in adipose SVF as measured by

gene expression (Fig. 1B). Likely additional SVF cell types also contribute to tissue BDNF. Since myeloid lineage cells are expressed in the brain, and BDNF has been shown to play a role in energy balance via CNS control of satiety, we also investigated whether our KO model affected BDNF expression in the hypothalamus. Gene expression of *Bdnf* in the hypothalamus did not differ between KO animals and their littermate controls (Fig. 1C). Physiological assessment using metabolic cages performed on KO animals and their littermate controls in the basal state revealed that KO mice had significantly lower energy expenditure (Fig. 1D) despite showing no difference in body weight or adiposity (Suppl. Fig. S1B).

KO mice have a blunted response to cold stimulation

Since a decrease in energy expenditure could be indicative of impaired sympathetic drive, we stimulated sympathetic nerve activity via cold exposure. When adult (22-23 week old) male mice were cold challenged at 5°C for 4 days, KO and control animals maintained similar body weight (Fig. 2A, left panel). However, KO animals had significantly increased adiposity (Fig. 2A, right panel). As cold exposure stimulates catecholamine-induced lipolysis mediated through sympathetic nerves, we next investigated innervation of the inguinal scWAT depot following a 7-day cold challenge. Protein expression of the pan-neuronal marker PGP9.5 was markedly reduced in inguinal scWAT of male KO mice compared to littermate controls (Fig. 2B, left panel). Protein expression of tyrosine hydroxylase (TH), a marker of sympathetic innervation and activation, was also drastically reduced in inguinal scWAT of KO animals compared to controls (Fig. 2B, right panel). Cold exposure induces expression of uncoupling protein 1 (UCP1) as required for adaptive thermogenesis, due to its ability to uncouple

the mitochondrial respiratory chain resulting in a proton leak and heat production. UCP1 is therefore a unique marker of BAT and browning in scWAT. Gene expression of *Ucp1* in inguinal scWAT of 7-day cold exposed mice was reduced in KO animals compared to littermate controls (Fig. 2C). Thyroid hormone potentiates SNS activation of thermogenesis in BAT but is produced via a distinct neuronal pathway from adipose sympathetic drive, and no changes in circulating thyroid hormones were observed between KO and CON animals (Fig. 2D). Histological assessment of inguinal scWAT revealed what appeared like increased multilocularity suggestive of browning in KO animals (Fig. 2E, Typogen Black staining). However, there was a striking lack of UCP1 expression in these areas in KO tissues (Fig. 2E). Considering denervation of WAT increases hyperplasia, the observed browning could more likely be areas in increased preadipocytes. Typogen Black (used here to reduce tissue autofluorescence) may also mark immune cells, thus there is potential for increased immune cell infiltration in the KO tissues as well. Taken together, these data suggested a “genetic denervation” of inguinal scWAT and diminished thermogenic response in inguinal scWAT in KO mice.

Genetic denervation of scWAT in LysM$^{cre/-}$:BDNF$^{fl/fl}$ (KO) mice is depot specific

We next sought to determine whether genetic denervation of scWAT in KO animals was restricted to adipose tissue or extended to other organs. BDNF is a known myokine, and muscle is an energy expending tissue. We assessed innervation of fast twitch (gastrocnemius) and slow twitch (soleus) muscle in CON and KO, by investigating occupancy of neuromuscular junctions (NMJs) at basal conditions in adult male mice. Immunostaining of the presynaptic nerve and vesicles (neurofilament and SV2, respectively), and postsynaptic acetylcholine receptors was performed to allow

visualization of NMJ (Suppl. Fig. S1C, left panel). Following counts of occupied, partially occupied, and unoccupied NMJs it was determined that there was no evidence of neurodegeneration in the NMJ of KO animals (Suppl. Fig. S1C, right panel). In the same animals we also assessed axon numbers of spinal (L5 ventral root), motor, and sensory nerves through cross-section imaging (Suppl. Fig. S1D). A lower axon count could reflect neuronal death, but no difference was observed between CON and KO animals.

Myeloid cells are also present in BAT tissue. We therefore wanted to evaluate whether a lack of BDNF in BAT myeloid cells would have an effect on this tissue's function. BAT of 7-day cold exposed 12-25 week old male CON and KO mice was evaluated. Protein expression of UCP1, TH, and PGP9.5 did not differ between KO mice and littermate controls (Suppl. Fig. S2A), which suggested BAT function was neither impaired nor was the tissue denervated. Histological assessment of BAT revealed no difference in cellular morphology, or UCP1 expression (Suppl. Fig. S2B). These results suggested that BDNF may not play a modulatory role in BAT innervation. Indeed, when adult male C57BL/6 mice were cold exposed or treated with the pharmacological β-3 adrenergic receptor (ADRβ3) agonist, CL316,243, no difference in BDNF secretion from BAT was observed when compared to basal conditions (Suppl. Fig. S2C). Together, these data supported scWAT depot specificity of our genetic denervation model, and BAT activation may simply be due to increased sympathetic nerve activity and not changes in neural plasticity in the tissue.

HFD feeding exacerbates fat mass accumulation in LysM$^{cre/-}$:BDNF$^{fl/fl}$ (KO) Mice

Loss of sympathetic innervation to inguinal scWAT has been shown to increase depot mass [46], however, in our genetic model of scWAT denervation, no difference in adiposity was observed under basal conditions (Suppl. Fig. S1A), despite the observed decrease in energy expenditure (Fig. 1D). We next metabolically challenged CON and KO mice with a 45% high fat diet (HFD). Adult (25 week old) male CON and KO mice were placed on a HFD for 3-11 weeks, to assess adipose integrity and energy balance. At 3 weeks of HFD feeding animals were characterized in metabolic cages. HFD resulted in only a slight decrease in energy expenditure in KO mice compared to littermate controls (Fig. 3A, top panel). However, KO mice showed a higher RER than CON animals during the light cycle, indicative of preferential metabolism of carbohydrates over lipids for fuel (Fig. 3A, bottom panel). These data fits with studies demonstrating that adipose nerves are important for lipolysis [47] and that denervation would shift fuel preference to carbohydrates. These physiological differences between CON and KO animals were observed despite no difference in food intake or change in body weight (Fig. 3B, top and bottom panels). After 6 weeks of HFD, KO mice displayed altered glucose control compared to CON animals (Fig. 3C), perhaps due to a shift in fuel utilization. By 11 weeks of HFD feeding, KO animals displayed greater adiposity than littermate controls (Fig. 3D). Taken together, the challenge of HFD feeding exacerbated fat accumulation in inguinal scWAT of KO animals and altered glucose utlization.

AAV-BDNF delivery increases innervation of scWAT

To test whether BDNF is capable of promoting scWAT innervation, we used adeno-associated virus (AAV) to deliver BDNF directly to the inguinal scWAT of two mouse

models that we have demonstrated to display adipose neuropathy [8]. The AS/Rec2 dual cassette vector used to deliver the BDNF transgene, transduces adipose tissue efficiently while restricting off-target transduction in liver [43]. Animals received a bolus injection of $1x10^{10}$ vg of AAV-BDNF in one unilateral inguinal scWAT depot and a vehicle injection in the contralateral inguinal scWAT. In BTBR MUT male mice at 16 weeks of age, when adipose neuropathy is prominent, protein expression of PGP9.5 was significantly increased after two weeks in the fat pads that received virus, compared to the vehicle treated depots (Fig. 4A, left panel). No difference was seen in protein expression of TH or PSD95 following AAV-BDNF treatment (Fig. 4A, right panels) for this dose and duration, in this neuropathic model. Using a HFD-induced model of neuropathy, AAV-BDNF delivery to unilateral scWAT similarly increased markers of innervation, but displayed a different trend than the *ob/ob* mice. A strong increase in TH and an increase in PSD95 were observed, with no significant increase in PGP9.5. Taken together, these data suggest a role for BDNF in promoting total innervation on inguinal scWAT.

Cold-induced neuroimmune cells (CINCs) are recruited to scWAT and express BDNF

After demonstrating the significance of myeloid derived BDNF to scWAT we sought to determine which myeloid cells were the source of BDNF. Given their multifaceted role in adipose tissue, being a source of BDNF in the brain (microglia), and the phenotype observed in a myeloid-lineage KO, we hypothesized that monocytes/macrophages were the leading source of BDNF in scWAT. Since previous studies indicated that BDNF is increased in scWAT with noradrenergic stimulation [8], CD11b+ F4/80+ macrophages were isolated from SVF of inguinal scWAT of room temperature and 5-day cold exposed

C57BL/6 adult (12 week old) male mice. *Bdnf* gene expression did not differ between room temperature and cold exposed CD11b+ F4/80+ macrophages (Fig. 4A). Although F4/80+ is considered a pan-macrophage marker, it was too broad to reveal subpopulation changes, and does not effectively mark monocytes (macrophage precursors), that could be infiltrating the tissue. Based on these findings we applied a different approach to determining which myeloid cells are the source of scWAT BDNF. Adult (12 week old) female control animals were maintained at room temperature or cold exposed for 10 days. Inguinal scWAT SVF was isolated and flow cytometrically analyzed using a custom antibody cocktail against immune cells. Surprisingly, cold exposure did not have an effect on either M1 or M2 ATMs (Fig 4B). Instead, the greatest increase was in Ly6c+ monocytes. Both Ly6C+ CCR2+ and Ly6C+ CCR2+ Cx3cr1+ populations increased in inguinal scWAT following cold exposure (Fig. 4C). Unbiased assessment using tSNE revealed subpopulations of immune cells changing in propensity in scWAT with cold, and between male and female mice (cold and room temperature). Interestingly, the Ly6C+ CCR2+ Cx3cr1+ population, which we call cold-induced neuroimmune cells (CINCs) increased in both male and female scWAT with cold (Fig. 4D).

To confirm that CCR2+ Cxc3cr1+ monocytes/macrophages were the source of BDNF, we FACS sorted out Ly6c+CCR2+Cx3cr1+ and Ly6c+CCR2+Cx3cr1- from inguinal scWAT SVF of 14 day cold exposed adult (12-13 week old) male C57BL/6 mice. Although the previously observed cold induced elevation of Ly6c+CCR2+Cx3cr1- in inguinal scWAT was not observed in the male cohort, Ly6c+CCR2+Cx3cr1+ did increase in response to cold (Fig. 4E). We measured *Bdnf* gene expression in cold induced Ly6c+CCR2+Cx3cr1+ (Cx3cr1+) cells and found that they showed a mild trend

for increased expression of *Bdnf* compared to cold exposed non-myeloid cells (Fig. 4F). Infiltration of more of these CINC cells to adipose upon cold exposure, and not an increase in per-cell BDNF levels, likely underlie the increased BDNF in adipose that was observed.

Adrβ3 gene expression in Cx3cr1+ cells confirmed the presence of norepinephrine (NE) receptor on these cells indicating the potential to be responsive to SNS stimulation (Suppl. Fig. S3), a likely mode for promoting BDNF release to the tissue. Taken together, these data indicated that Cx3cr1+ cells are cold-induced neuroimmune cells (CINCs) that have the potential to be stimulated by sympathetic nerves, and express BDNF.

Discussion

Here we present evidence of the necessity for myeloid-derived BDNF in maintaining inguinal scWAT innervation. Loss of BDNF from LysM+ myeloid cells resulted in a severe decrease in total innervation of the inguinal adipose tissue as measured by the pan-neuronal marker PGP9.5, and a near complete denervation of sympathetic nerves (as measured by TH protein expression. We attribute this ‘genetic denervation’ as a cause for the observed decrease in energy expenditure exhibited under basal conditions, impaired thermogenic potential evidenced by lack of UCP1 induction and impaired lipolysis in WAT during cold stimulation, and worsened response to HFD. These phenotypes fit with the known roles of adipose nerves in regulating proper adipogenesis, lipolysis, thermogenesis and overall metabolic health in adipose tissues.

Diet-induced obesity results in chromic low grade adipose inflammation due to infiltration of pro-inflammatory immune cells to the tissue, and ATM content increase from 10-15% (in lean mice) to ~50% [31, 48]. In addition, phenotypic switching of CD4+ T cells and recruitment of T cell and B cells precedes macrophage infiltration, and macrophage polarity is affected to exhibit a more inflammatory phenotype.

We initially hypothesized that anti-inflammatory (M2) ATMs were the source of scWAT BDNF. However, we observed no changes in M1 or M2 populations in scWAT after cold exposure. Instead we saw an increase in Ly6c+CCR2+Cx3cr1+ monocytes in both male and female mice. We have named these cells CINCs since they are recruited to scWAT by cold, and express BDNF. Surprisingly, it would appear that CINCs are a pro-inflammatory cell type as Ly6C+ is a marker of inflammatory monocytes. Although pro-inflammatory cell infiltration to adipose tissue is usually a harbinger of metabolic dysfunction, an acute inflammatory response is necessary in wound healing and tissue remodeling. By utilizing an unbiased 20 antibody labeling approach to assessing adipose SVF, we have discovered subsets of myeloid cells that respond to environmental stimuli providing further granularity to the myriad of immune cells types active in adipose.

Recently, a Cx3cr1+ population of macrophages had been described in association with sympathetic nerves in adipose tissue [49]. These sympathetic nerve associated macrophages (SAMs) were found to regulate catecholamine levels on adipose tissue by phagocytosing and degrading norepinephrine (NE) [49]. Whether SAMs are the same cells as our CINCs remains uncertain, as other distinguishing markers like Ly6C and CCR2 were not assessed in both studies. Similar to CINCs, SAMs *do* exhibit pro-inflammatory markers. SAMs hone to WAT in the obese state but

conversely we see CINCs hone to WAT with cold/noradrenergic-stimulation, indicating the two immune populations may have opposing roles, including potential for phagocytosing nerve debris or stimulating nerve regeneration respectively. Fitting with this, SAMs sequester and degrade NE, while CINCs express BDNF. One could speculate then, that SAMs serve to decrease SNS input to the tissue while CINCs serve to increase innervation of WAT. On the other hand, Cx3cr1+ macrophages have been shown to play diverse and even opposing roles in the intestines [50], a phenotypic plasticity which may also be present in adipose tissue. One thing that is clear is that the M1/M2 paradigm of ATM classification is an oversimplification of the functionally distinct populations of macrophages active in adipose tissue. However, further markers beyond Cx3cr1+ are necessary to fully understand and phenotype the rich variety of macrophages in adipose. Compounding the difficulty in clearly delineating macrophage populations is that macrophage activation is a dynamic process. Phenotypic switching appears to be sequential, responding to microenvironment stimuli [51] and may be dependent on spatiotemporal differences in tissue resident immune cell subtypes [52].

We postulate that CINCs contribute to nerve remodeling under noradrenergic stimulation, leading to BDNF release. Cao, et al have recently suggested that sympathetic nerve plastically is dependent on cold-induced, adipose-derived NGF [53]. Although they provide evidence that NGF is involved to some degree in promoting cold induced sympathetic nerve density and browning of scWAT, there is insufficient evidence as to the cellular source of NGF (our data indicate it is produced more by mature adipocytes than SVF cells, and thus may be promoting innervation of the adipocytes and not the SVF). After determining that NGF gene expression increased in the first couple of days of cold exposure, Cao, et al used an NGF neutralizing antibody

to prevent NGF activity and observed decreased sympathetic nerve density in response to cold. Several caveats to this study exist since cold-induced sympathetic nerve density was not assessed in the whole adipose depot, and we know that regional innervation patterns exist from our previous works as well as others [54]. Furthermore, NGF neutralizing antibody was administered systemically, and there was no control for off-target effects, including any that may have affected hypothalamic control of sympathetic drive to scWAT. However, their approach in preventing TrkA receptor function in adipose nerves and showing decreased browning and sympathetic nerve density lends credence to the notion that NGF plays a role in adipose innervation, similar to the role we observe for BDNF, and taken together it is clear that locally-derived nerve growth factors are important for maintaining proper brain-adipose communication and adipose innervation. Considering the variety of NFs and the multitude of cell types in adipose tissue it would not be surprising if both NGF and BDNF play a role in adipose innervation through different mechanisms, and the presence of one NFs within as tissue does not have to preclude the physiological role of another. Promoting innervation of a specific axonal subtype to a specific cell in the tissue may in fact be accomplished by coordinated secretion of a given growth factor by the target cell type; whereby mature adipocytes secrete NGF and SVF immune cells secrete BDNF.

Acknowledgements

The authors wish to thank the following individuals from University of Maine: Brenda Kennedy-Wade and Prof. James Weber for assistance in the animal facility, Dawna Beane for paraffin embedding, Callie Greco, Cameron Fudge, and Sarah Berez for animal care. The authors also wish to thank Drs. Gregory Cox and Robert Burgess for sharing their NMJ assessment methods; and Nicholas Cutter and Emma Bragdon for help with spinal, motor, and sensory nerve assessments.

Funding

For this project, the Townsend Lab was funded by start-up funds from the Office of the Vice President for Research at University of Maine, a Rising Tide Seed Grant from University of Maine, a Junior Faculty Award from the American Diabetes Association, and an R01 from NIH NIDDK. The Godwin lab is supported by a NIH COBRE award (P20GM104318).

Author Contributions

MB designed experiments, analyzed data, and wrote the manuscript. EW and SK collected and analyzed histology data. SK and RA collected and analyzed data related to brown adipose tissue. JW analyzed histology data. WH and LC produced and provided AAV-BDNF. JG conducted the flow cytometric analysis on adipose immune cells. KLT designed experiments, analyzed data, conceived of and oversaw the project, and wrote the manuscript. KLT is the guarantor of this work and, as such, had full

access to all the data in the study and takes responsibility of the data and the accuracy of the data analysis.

Conflict of Interest Statement/Duality

The authors do not have any conflicts of interest to disclose.

Figure Legends

Figure 1. BDNF is expressed in the SVF of adipose; *LysM$^{cre/-}$:BDNF$^{fl/fl}$* (KO) mice have lower energy expenditure. Adult male CB57/BL6 mice were cold exposed at 5°C and SVF was isolated from mature adipocytes of the inguinal scWAT depot. Differences in gene expression between adipose compartments of neurotrophic factors, *Bdnf, Ngf,* and *Vegfa,* is shown (A). Data analyzed by Student's t-test, two-tailed, N=4. BDNF gene expression in adipose SVF of *LysM$^{-/-}$:BDNF$^{fl/fl}$* (CON) versus *LysM$^{cre/-}$:BDNF$^{fl/fl}$* (KO) mice (B). Data analyzed by Student's t-test, two-tailed, N=4 per group. Gene expression of *Bdnf* in hypothalamus of *LysM$^{-/-}$:BDNF$^{fl/fl}$* (CON) versus *LysM$^{cre/-}$:BDNF$^{fl/fl}$* (KO) mice (C). Data analyzed by Student's t-test, two-tailed, N=5 CON; N=6 KO. Adult (8-12 week old) male CON and KO mice were assessed in metabolic cages (CLAMS). Waveform analysis of metabolic cage measurements taken at 15min increments for 48 hrs (D). Time of day is indicated on the x-axis, animals were maintained on a 12 hr light/dark cycle (black bars indicate dark cycle). KO mice displayed lower energy expenditure represented as heat calculated from measures of VO_2 and VCO_2 over the whole 24hr (D). For all error bars are SEMs.

Figure 2. *LysM$^{cre/-}$:BDNF$^{fl/fl}$* (KO) have increased adiposity and impaired response to cold due to genetic denervation of scWAT. Adult (22-23 week old) male *LysM$^{-/-}$:BDNF$^{fl/fl}$* (CON) and *LysM$^{cre/-}$:BDNF$^{fl/fl}$* (KO) mice were cold exposed at 5°C for 4 days; body weight and adiposity were compared between CON and KO groups (A). Body and tissue weight data were analyzed by two-tailed Student's T-Test, N=5 CON, N=8 KO. Protein expression of PGP9.5 and tyrosine hydroxylase (TH) in inguinal scWAT was measured by western blotting from adult (12-25 week old) 7-day cold (5°C) exposed WT/CON and KO male animals (B). β-tubulin was used as a loading control for normalization. Data were analyzed by two-tailed Student's T-Test, N=3 WT/CON, N=4 KO, * denotes data that was removed from analysis due to lack of expression of loading control. Gene expression of *Ucp1* was measured in adult (12-25 week old) 7-day cold (5°C) exposed WT/CON and KO males (C). Data were analyzed by two-tailed Student's T-Test, N=5 WT/CON, N=5 KO. Circulating thyroid hormones, thyroxine (T4) and triiodothyronine (T3), were measured by ELISA from serum of adult (22-23 week old) 4-day cold (5°C) exposed CON and KO male mice (D). Data were analyzed by One-way ANOVA, with Tukey's multiple comparisons test, N=5 CON, N=8 KO. Immunofluorescent staining for UCP1 was performed on inguinal scWAT sections of adult (22-23 week old) male CON and KO mice following 4-day cold (5°C) exposure (E). Typogen Black, used to quench lipid autofluorescence, provided staining cell morphology which was visualized under brightfield microscopy. Images were acquired with a 10X objective for a total magnification of 100X, and are representative of N=5 CON, N=8 KO. For all error bars are SEMs.

Figure 3. *LysM$^{cre/-}$:BDNF$^{fl/fl}$* (KO) showed accelerated fat accumulation on an 45% HFD. Adult (25 week old) male *LysM$^{-/-}$:BDNF$^{fl/fl}$* (CON) and *LysM$^{cre/-}$:BDNF$^{fl/fl}$* (KO) were challenged with a 45% HFD for 3 weeks before undergoing physiological assessment in metabolic cages (A). Energy expenditure as measured by heat was lower for KO versus CON only for a short period during the dark cycle (A, top panel). Respiratory exchange as a ratio (RER) between the two groups, indicated greater use of carbohydrates for fuel by KO animals during the light cycle. Data presented as waveform analysis of measurements taken at 15min increments for 3 days. Time of day is indicated on the x-axis, and animals were maintained on a 12 hr light/dark cycle (black bars indicate dark cycle)**.** Data analyzed by two-way repeated measures ANOVA with Fisher's LSD test; N=4 per group. Adult (25 week old) male CON and KO animals were placed on a 45% HFD, daily food intake (represented as cumulative food intake) (B, top panel) was measured for the first week of HFD feeding. Percent change in body weight (B, bottom panel) was measured for the first 7 days of HFD feeding. Data were analyzed by two-tailed Student's T-Test, N=6 CON, N=4 KO. Glucose tolerance testing was performed at 6 weeks of HFD feeding (C). Data were analyzed by Two-way ANOVA, with Tukey's multiple comparisons test, N=4 CON, N=4 KO. Adiposity was measured for CON and KO animals after 11 weeks of HFD feeding as a percentage of scWAT over body weight (D). Data were analyzed by two-tailed Student's T-Test, N=4 CON, N=4 KO. For all error bars are SEMs. *$p < 0.05$, **$p < 0.01$, ***$p < 0.001$, ****$p < 0.0001$.

Figure 4. AVV-BDNF delivery re-innervated inguinal adipose tissue. Adult (16 week old) male BTBR$^{ob/ob}$ (Mutant) mice (N=3) received single injection of AAV-BDNF ($1x10^{10}$ vg) into their left inguinal scWAT and an equal volume of vehicle into their right inguinal scWAT; protein expression of PGP9.5, TH, and PSD95 in inguinal scWAT was measured by western blotting after 2 weeks (A). Adult (11-13 week old) male C57BL/6 mice were placed on a 58% HFD for 17 weeks to induce neuropathy. Following dietary intervention animals (N=6) received single injection of AAV-BDNF ($1x10^{10}$ vg) into their left inguinal scWAT and an equal volume of vehicle into their right inguinal scWAT; protein expression of PGP9.5, TH, and PSD95 in inguinal scWAT was measured by western blotting after 2 weeks (B). Protein expression was normalized to β-tubulin or Cyclophilin B, band intensity was quantified in Image J and analyzed by two-tailed Student's T-Test; error bars are SEMs.

Figure 5. Cold induced neuroimmune cells (CINCs) hone in to inguinal scWAT and express *Bdnf*. Adult (12 week old) male C57BL/6 were either maintained at room temperature (RT) or cold exposed (5°C) for 5 days, ATMs from inguinal scWAT depots were isolated using magnetic-activated cell sorting (MACS) by positive selection of CD11b+ followed by F4/80+ cells. *Bdnf* gene expression in doubly labeled CD11b+ F4/80+ macrophages was compared between RT and cold exposed animals (A). Data were analyzed by two-tailed Student's T-Test, N=4 per group. Adult (12 week old) female control animals were either maintained at room temperature (RT) or cold exposed (5°C) for 10 days, SVF from bilateral inguinal scWAT was isolated and FACS sorted using a 20 cell surface marker panel for myeloid lineage immune cells (B-C). Changes in M1/M2 polarity (B) and Ly6C+ macrophage precursors/monocytes (C) were measured between RT and cold exposed animals. Data were analyzed by two-tailed Student's T-Test, N=3 per groups. Adult male (M) and female (F) control animals were either maintained at room temperature (RT) or cold exposed (5°C) for 10 days, SVF from bilateral inguinal scWAT was isolated and FACS sorted using a 20 cell surface marker panel for myeloid lineage immune cells (N=5 per group). t-Distributed Stochastic Neighbor Embedding (tSNE) analysis was performed to identify myeloid lineage cell population changes in response to cold exposure; Ly6c+CCR2+ and Ly6c+CCR2+Cx3cr1+ were identified as adipose cold induced neuroimmune cells (CINCs) (D). Adult (12-13 week old) male C57BL/6 were either maintained at room temperature (RT) or cold exposed (5°C) for 14 days; SVF from bilateral inguinal scWAT was isolated and FACS sorted (E-F). Previously identified CINCs, Ly6c+CCR2+Cx3cr1- and Ly6c+CCR2+Cx3cr1+ cells were compared between RT and cold exposed animals

(E). *Bdnf* gene expression was measured in Ly6c+CCR2+Cx3cr1+ cells (F). Data analyzed by two-tailed Student's T-Test, N=4 per group. For all error bars are SEMs. *p < 0.05, **p < 0.01, ***p < 0.001, ****p < 0.0001.

References

1. Dulloo, A.G. and D.S. Miller, *Energy balance following sympathetic denervation of brown adipose tissue*. Can.J Physiol.Pharmacol., 1984. **62**(2): p. 235-240.
2. Minokoshi, Y., M. Saito, and T. Shimazu, *Sympathetic denervation impairs responses of brown adipose tissue to VMH stimulation.* Am J Physiol., 1986. **251**(5 Pt 2): p. R1005-R1008.
3. Desautels, M., R.A. Dulos, and B. Mozaffari, *Selective loss of uncoupling protein from mitochondria of surgically denervated brown adipose tissue of cold-acclimated mice.* Biochem.Cell Biol., 1986. **64**(11): p. 1125-1134.
4. Dulloo, A. and D. Miller, *Energy balance following sympathetic denervation of brown adipose tissue.* Canadian journal of physiology and pharmacology, 1984. **62**(2): p. 235-240.
5. Bowers, R.R., et al., *Sympathetic innervation of white adipose tissue and its regulation of fat cell number.* American Journal of Physiology-Regulatory, Integrative and Comparative Physiology, 2004. **286**(6): p. R1167-R1175.
6. Foster, M.T. and T.J. Bartness, *Sympathetic but not sensory denervation stimulates white adipocyte proliferation.* Am J Physiol Regul Integr Comp Physiol, 2006. **291**(6): p. R1630-7.
7. Harris, R.B., *Sympathetic denervation of one white fat depot changes norepinephrine content and turnover in intact white and brown fat depots.* Obesity.(Silver.Spring). 2012: p. 10.
8. Blaszkiewicz, M., et al., *Neuropathy and neural plasticity in the subcutaneous white adipose depot.* PLoS One, 2019. **14**(9): p. e0221766.
9. Gray, J.D., T.A. Milner, and B.S. McEwen, *Dynamic plasticity: the role of glucocorticoids, brain-derived neurotrophic factor and other trophic factors.* Neuroscience, 2013. **239**: p. 214-27.
10. Terenghi, G., *Peripheral nerve regeneration and neurotrophic factors.* J Anat, 1999. **194 (Pt 1)**: p. 1-14.
11. An, J.J., et al., *Distinct role of long 3' UTR BDNF mRNA in spine morphology and synaptic plasticity in hippocampal neurons.* Cell, 2008. **134**(1): p. 175-87.
12. Kleim, J.A., et al., *BDNF val66met polymorphism is associated with modified experience-dependent plasticity in human motor cortex.* Nat Neurosci, 2006. **9**(6): p. 735-7.
13. Fritsch, B., et al., *Direct current stimulation promotes BDNF-dependent synaptic plasticity: potential implications for motor learning.* Neuron, 2010. **66**(2): p. 198-204.
14. Tapia-Arancibia, L., et al., *Physiology of BDNF: focus on hypothalamic function.* Front Neuroendocrinol, 2004. **25**(2): p. 77-107.
15. Unger, T.J., et al., *Selective deletion of Bdnf in the ventromedial and dorsomedial hypothalamus of adult mice results in hyperphagic behavior and obesity.* J Neurosci, 2007. **27**(52): p. 14265-74.
16. Nakagawa, T., et al., *Brain-derived neurotrophic factor regulates glucose metabolism by modulating energy balance in diabetic mice.* Diabetes, 2000. **49**(3): p. 436-44.
17. Nonomura, T., et al., *Brain-derived neurotrophic factor regulates energy expenditure through the central nervous system in obese diabetic mice.* Int J Exp Diabetes Res, 2001. **2**(3): p. 201-9.
18. Xu, B., et al., *Brain-derived neurotrophic factor regulates energy balance downstream of melanocortin-4 receptor.* Nat Neurosci, 2003. **6**(7): p. 736-42.

19. Xu, B. and X. Xie, *Neurotrophic factor control of satiety and body weight.* Nat Rev Neurosci, 2016. **17**(5): p. 282-92.
20. Sornelli, F., et al., *Adipose tissue-derived nerve growth factor and brain-derived neurotrophic factor: results from experimental stress and diabetes.* Gen Physiol Biophys., 2009. **28 Spec No:179-83.**: p. 179-183.
21. Hausman, G.J., et al., *Secreted proteins and genes in fetal and neonatal pig adipose tissue and stromal-vascular cells.* J Anim Sci, 2006. **84**(7): p. 1666-81.
22. Bernhard, F., et al., *Functional relevance of genes implicated by obesity genome-wide association study signals for human adipocyte biology.* Diabetologia, 2013. **56**(2): p. 311-22.
23. Nakagomi, A., et al., *Role of the central nervous system and adipose tissue BDNF/TrkB axes in metabolic regulation.* NPJ Aging Mech Dis, 2015. **1**: p. 15009.
24. Goss, J.R., et al., *Astrocytes are the major source of nerve growth factor upregulation following traumatic brain injury in the rat.* Exp Neurol, 1998. **149**(2): p. 301-9.
25. Madduri, S. and B. Gander, *Schwann cell delivery of neurotrophic factors for peripheral nerve regeneration.* J Peripher Nerv Syst, 2010. **15**(2): p. 93-103.
26. Leon, A., et al., *Mast cells synthesize, store, and release nerve growth factor.* Proc Natl Acad Sci U S A, 1994. **91**(9): p. 3739-43.
27. Kobayashi, H., et al., *Human eosinophils produce neurotrophins and secrete nerve growth factor on immunologic stimuli.* Blood, 2002. **99**(6): p. 2214-20.
28. Noga, O., et al., *The production, storage and release of the neurotrophins nerve growth factor, brain-derived neurotrophic factor and neurotrophin-3 by human peripheral eosinophils in allergics and non-allergics.* Clin Exp Allergy, 2003. **33**(5): p. 649-54.
29. Lambiase, A., et al., *Human CD4+ T cell clones produce and release nerve growth factor and express high-affinity nerve growth factor receptors.* Journal of Allergy and Clinical Immunology, 1997. **100**(3): p. 408-414.
30. Kerschensteiner, M., et al., *Activated human T cells, B cells, and monocytes produce brain-derived neurotrophic factor in vitro and in inflammatory brain lesions: a neuroprotective role of inflammation?* Journal of Experimental Medicine, 1999. **189**(5): p. 865-870.
31. Weisberg, S.P., et al., *Obesity is associated with macrophage accumulation in adipose tissue.* J Clin Invest, 2003. **112**(12): p. 1796-1808.
32. Winer, D.A., et al., *B cells promote insulin resistance through modulation of T cells and production of pathogenic IgG antibodies.* Nat Med, 2011. **17**(5): p. 610-7.
33. Rausch, M.E., et al., *Obesity in C57BL/6J mice is characterized by adipose tissue hypoxia and cytotoxic T-cell infiltration.* Int J Obes (Lond), 2008. **32**(3): p. 451-63.
34. Elgazar-Carmon, V., et al., *Neutrophils transiently infiltrate intra-abdominal fat early in the course of high-fat feeding.* J Lipid Res, 2008. **49**(9): p. 1894-903.
35. Liu, J., et al., *Genetic deficiency and pharmacological stabilization of mast cells reduce diet-induced obesity and diabetes in mice.* Nat.Med, 2009. **15**(8): p. 940-945.
36. Strissel, K.J., et al., *T-cell recruitment and Th1 polarization in adipose tissue during diet-induced obesity in C57BL/6 mice.* Obesity (Silver Spring), 2010. **18**(10): p. 1918-25.
37. Grant, R., et al., *Quantification of adipose tissue leukocytosis in obesity.* Methods Mol Biol, 2013. **1040**: p. 195-209.
38. Hui, X., et al., *Adiponectin Enhances Cold-Induced Browning of Subcutaneous Adipose Tissue via Promoting M2 Macrophage Proliferation.* Cell Metab, 2015. **22**(2): p. 279-90.
39. Rost, B., et al., *Monocytes of allergics and non-allergics produce, store and release the neurotrophins NGF, BDNF and NT-3.* Regul Pept, 2005. **124**(1-3): p. 19-25.

40. Parkhurst, C.N., et al., *Microglia promote learning-dependent synapse formation through brain-derived neurotrophic factor.* Cell, 2013. **155**(7): p. 1596-609.
41. Lai, S.W., et al., *Regulatory Effects of Neuroinflammatory Responses Through Brain-Derived Neurotrophic Factor Signaling in Microglial Cells.* Mol Neurobiol, 2018. **55**(9): p. 7487-7499.
42. Gemma, C. and A.D. Bachstetter, *The role of microglia in adult hippocampal neurogenesis.* Front Cell Neurosci, 2013. **7**: p. 229.
43. Huang, W., et al., *Targeting Visceral Fat by Intraperitoneal Delivery of Novel AAV Serotype Vector Restricting Off-Target Transduction in Liver.* Mol Ther Methods Clin Dev, 2017. **6**: p. 68-78.
44. Liu, X., et al., *Adipose tissue insulin receptor knockdown via a new primate-derived hybrid recombinant AAV serotype.* Mol Ther Methods Clin Dev, 2014. **1**.
45. Obrosova, I.G., et al., *High-fat diet induced neuropathy of pre-diabetes and obesity: effects of "healthy" diet and aldose reductase inhibition.* Diabetes, 2007. **56**(10): p. 2598-608.
46. Bartness, T.J. and C.K. Song, *Brain-adipose tissue neural crosstalk.* Physiol Behav., 2007. **91**(4): p. 343-351.
47. Bartness, T.J., et al., *Neural innervation of white adipose tissue and the control of lipolysis.* Front Neuroendocrinol., 2014. **35**(4): p. 473-493.
48. Xu, H., et al., *Chronic inflammation in fat plays a crucial role in the development of obesity-related insulin resistance.* J Clin Invest, 2003. **112**(12): p. 1821-1830.
49. Pirzgalska, R.M., et al., *Sympathetic neuron–associated macrophages contribute to obesity by importing and metabolizing norepinephrine.* Nature medicine, 2017. **23**(11): p. 1309.
50. Regoli, M., et al., *The Multifaceted Personality of Intestinal CX3CR1(+) Macrophages.* Trends Immunol, 2017. **38**(12): p. 879-887.
51. Stout, R.D., et al., *Macrophages sequentially change their functional phenotype in response to changes in microenvironmental influences.* J Immunol, 2005. **175**(1): p. 342-9.
52. Lumeng, C.N., et al., *Phenotypic switching of adipose tissue macrophages with obesity is generated by spatiotemporal differences in macrophage subtypes.* Diabetes, 2008. **57**(12): p. 3239-3246.
53. Cao, Y., H. Wang, and W. Zeng, *Whole-tissue 3D imaging reveals intra-adipose sympathetic plasticity regulated by NGF-TrkA signal in cold-induced beiging.* Protein Cell, 2018. **9**(6): p. 527-539.
54. Chi, J., et al., *Three-Dimensional Adipose Tissue Imaging Reveals Regional Variation in Beige Fat Biogenesis and PRDM16-Dependent Sympathetic Neurite Density*. Cell Metab, 2018. **27**(1): p. 226-236 e3.

Figure 1

A. **Gene Expression of Neurotrophic Factors in Adipose Compartments**

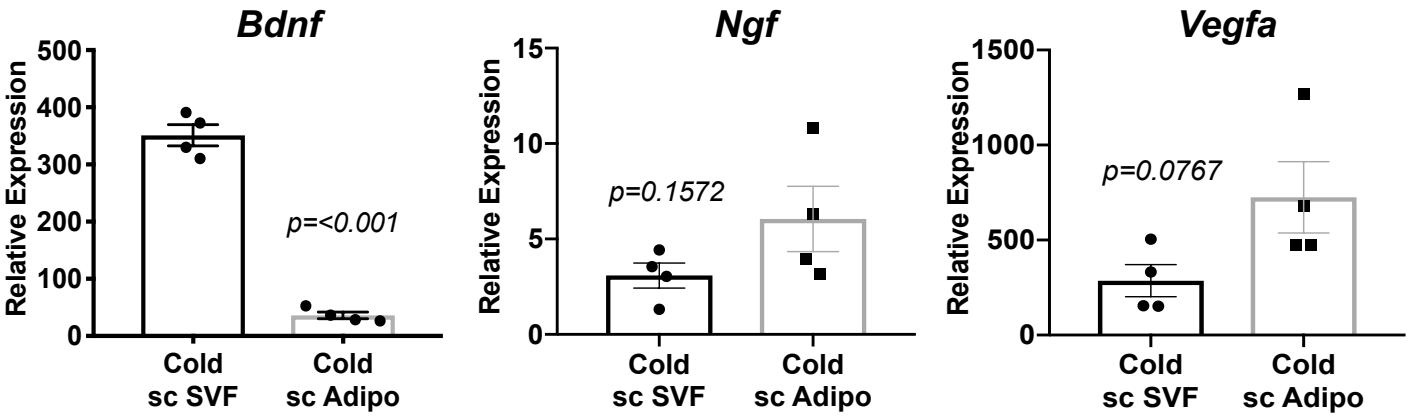

B. **BDNF Gene Expression in Inguinal scWAT SVF of *LysMCre:BDNF*$^{-/-}$ (KO) mice**

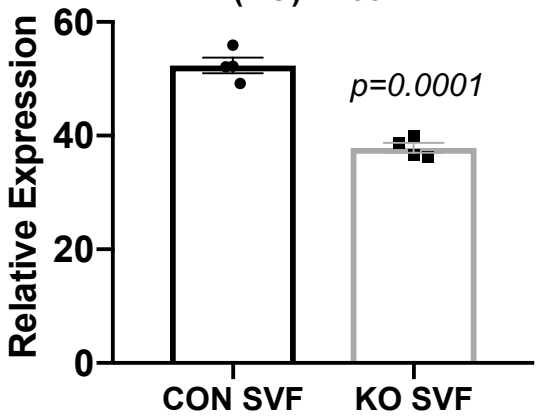

C. **BDNF Gene Expression in Hypothalamus of *LysMCre:BDNF*$^{-/-}$ (KO) mice**

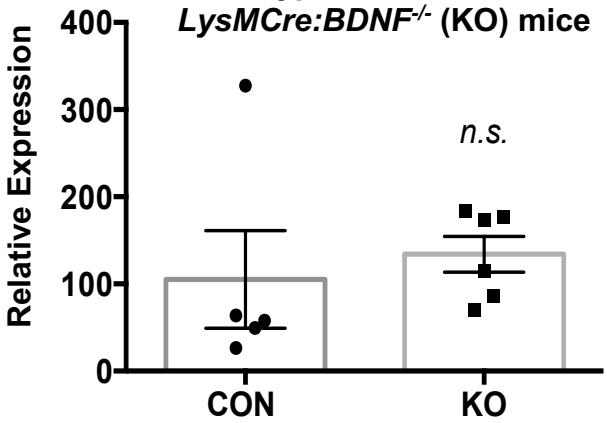

D. **Basal Heat (CLAMS)**

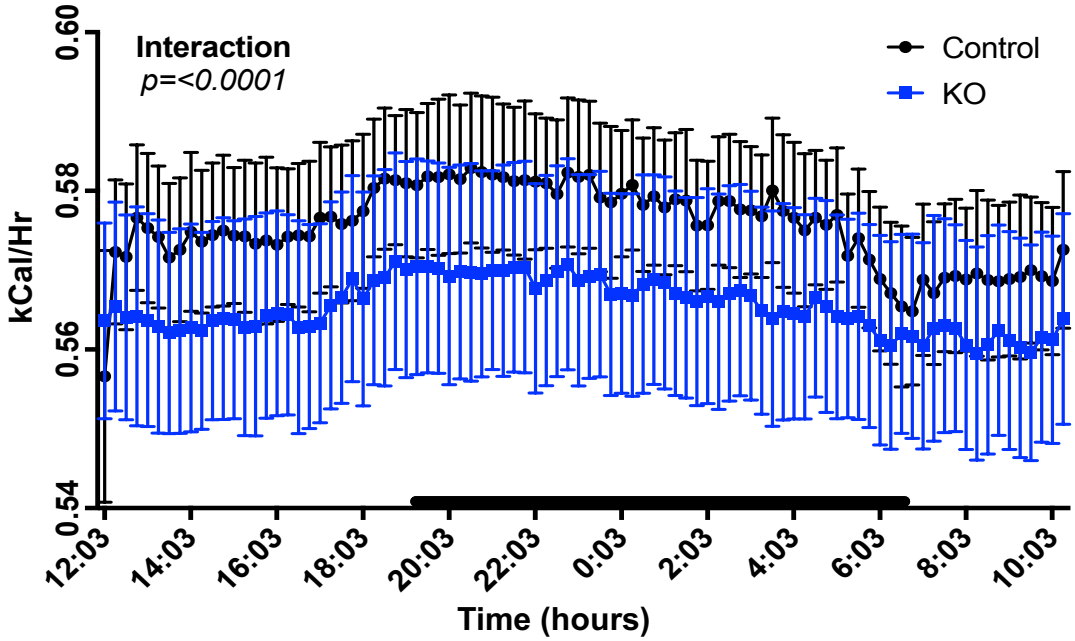

Figure 2

A.

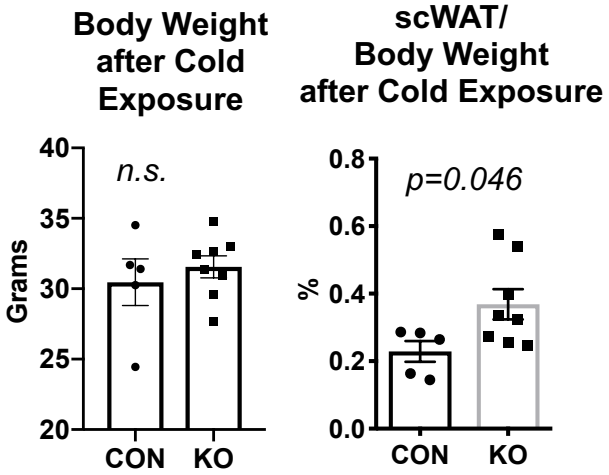

B. **Inguinal scWAT Innervation after Cold Exposure**

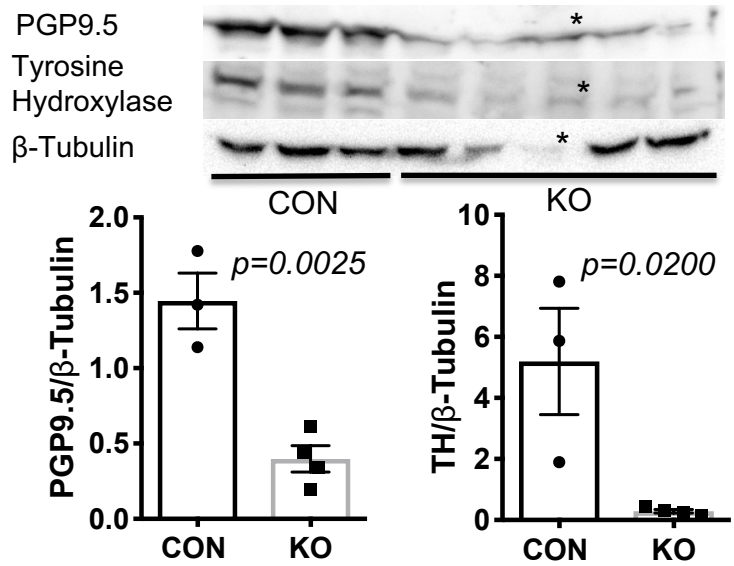

C.

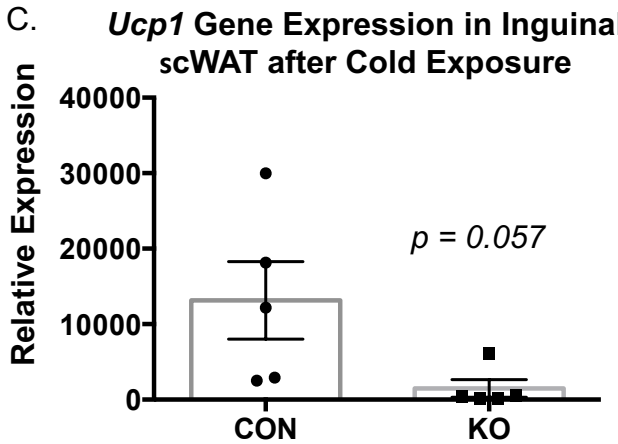

D.

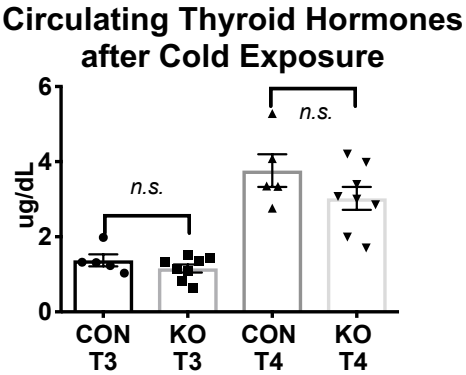

E. **Histology and UCP1 Protein in Inguinal scWAT Following Cold Exposure**

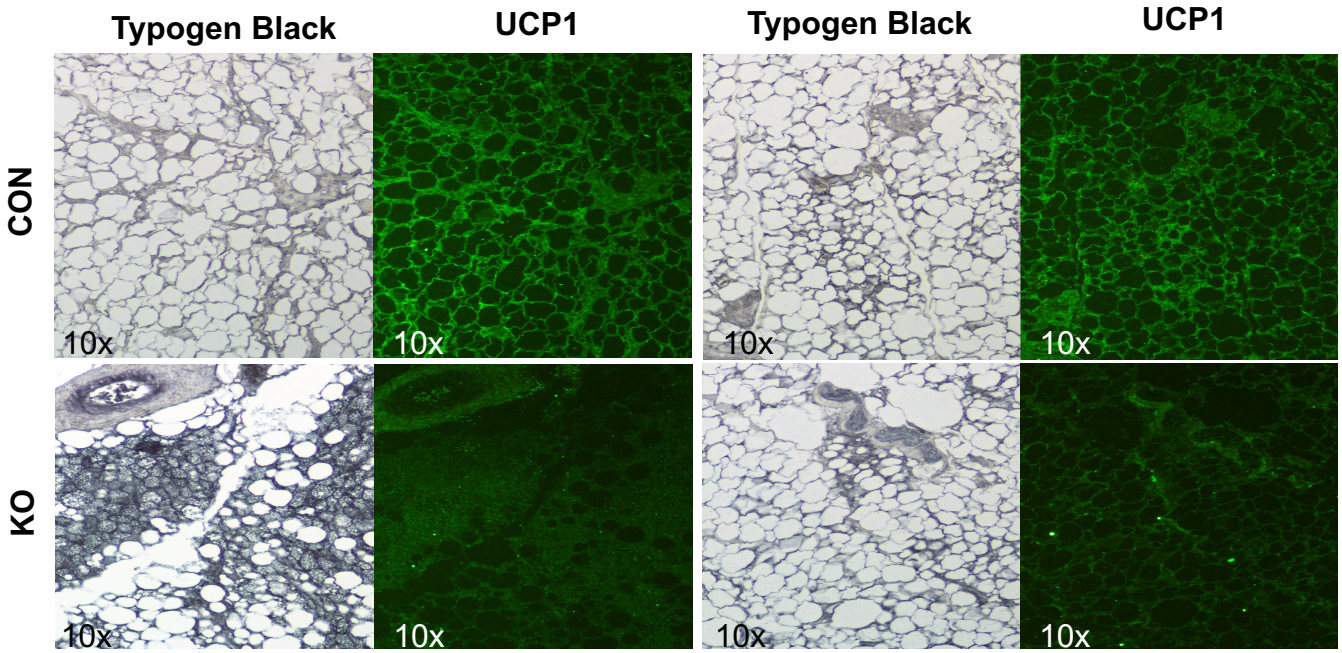

Figure 3

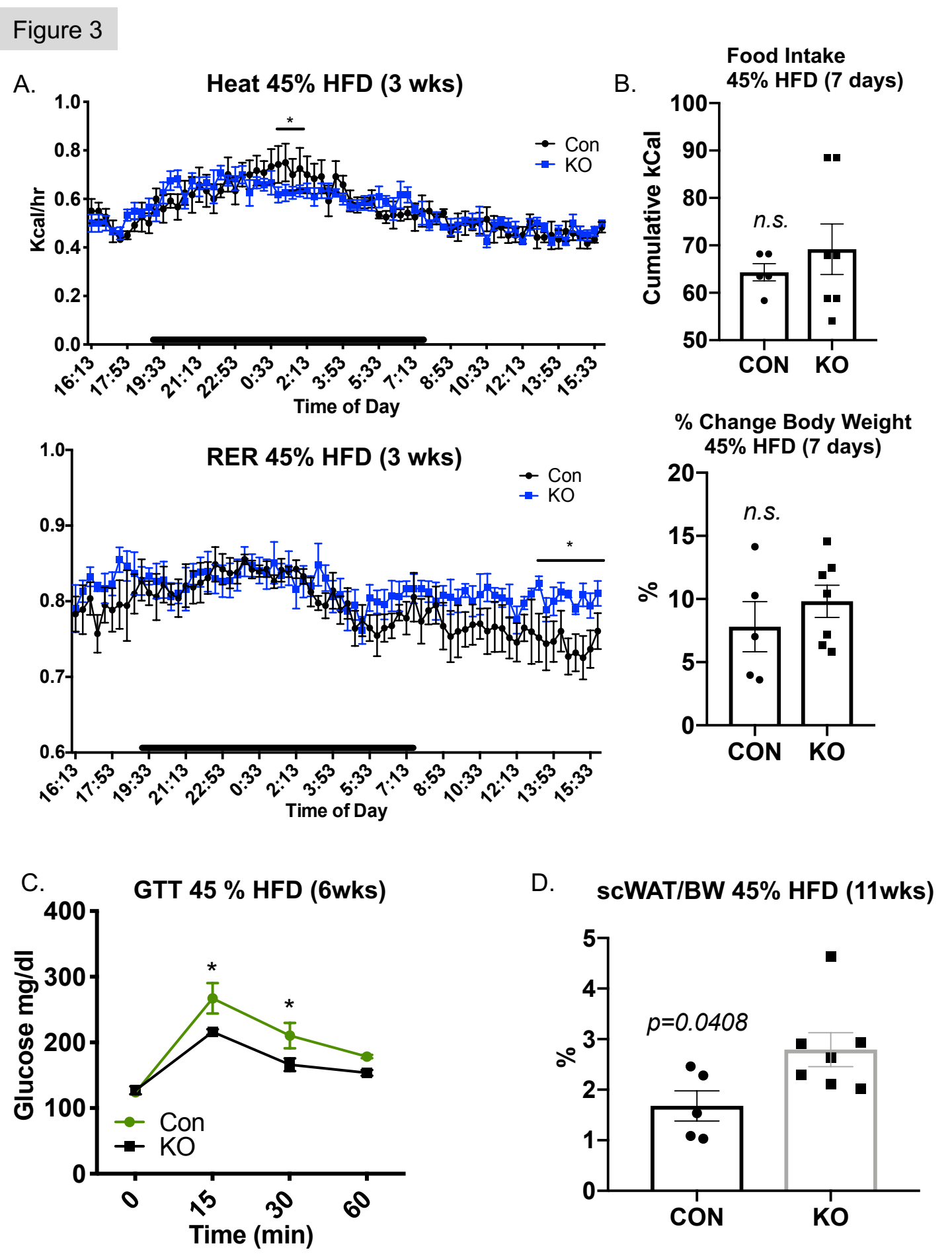
A.
Heat 45% HFD (3 wks)
Kcal/hr
Time of Day
Con
KO
RER 45% HFD (3 wks)
B.
Food Intake
45% HFD (7 days)
Cumulative kCal
n.s.
CON
KO
% Change Body Weight
45% HFD (7 days)
%
C.
GTT 45 % HFD (6wks)
Glucose mg/dl
Time (min)
D.
scWAT/BW 45% HFD (11wks)
p=0.0408

Figure 4

A. **AAV-BDNF Delivery to Adipose of BTBR *ob/ob* Mice**

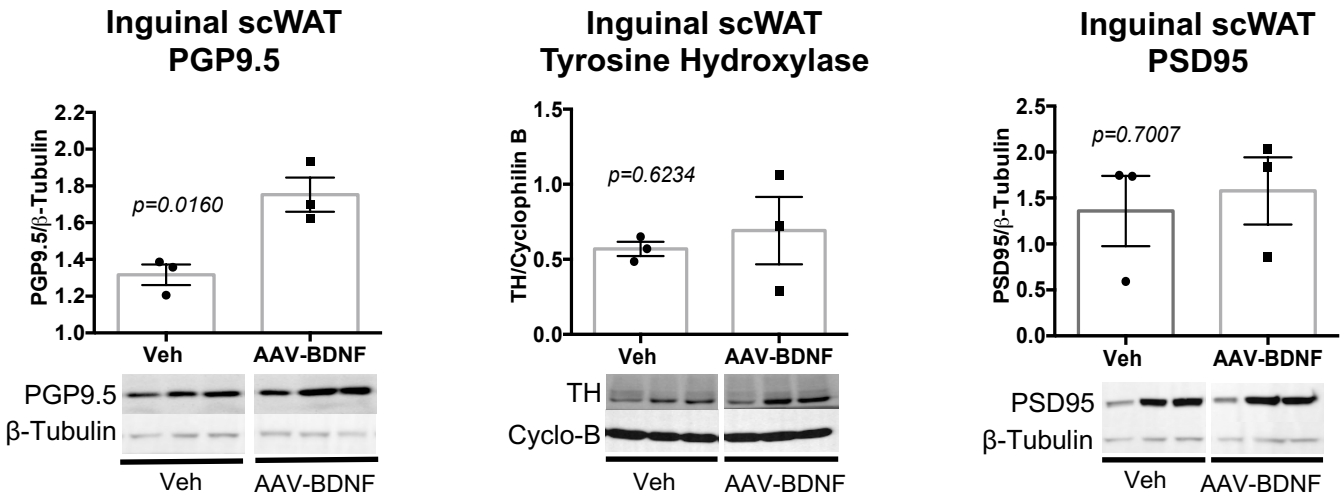

B. **AAV-BDNF Delivery to Adipose of HFD-Induced Neuropathy Mice**

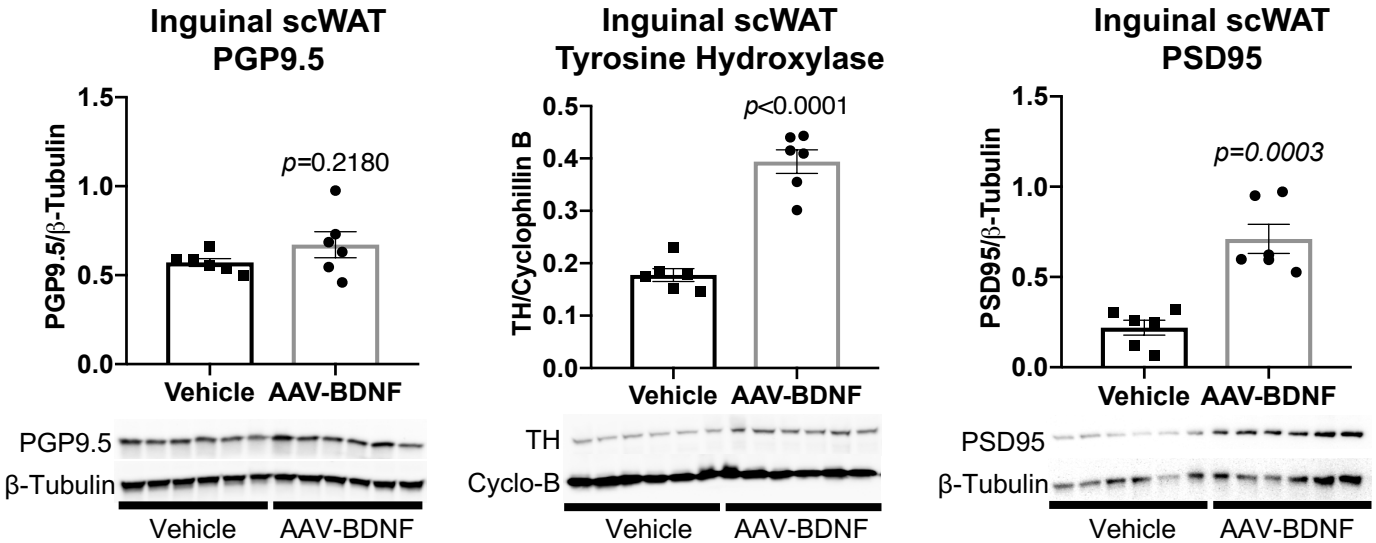

Figure 5

A. ***Bdnf* Gene Expression in F4/80⁺ Macrophages**

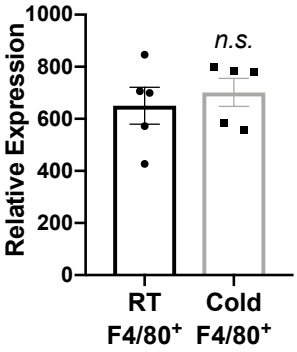

B. **Macrophage polarity**

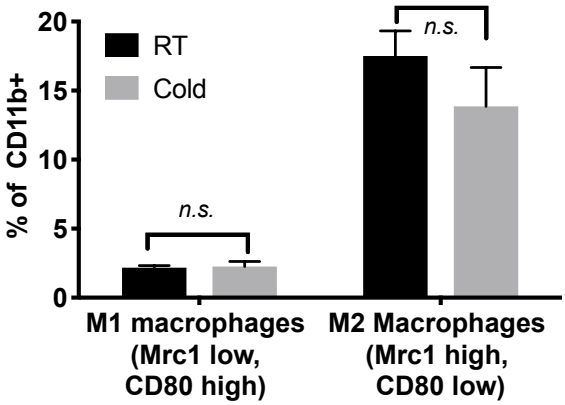

C. **Monocyte changes**

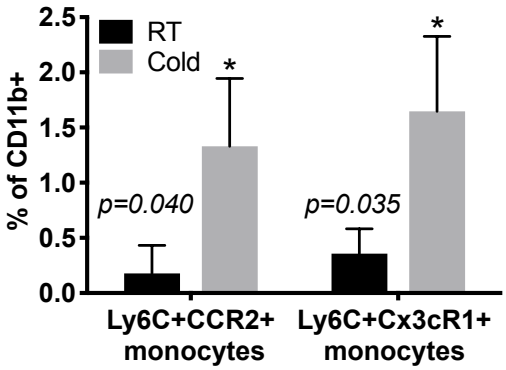

D. **tSNE Analysis of Male/Female Cold Induced Immune Changes in Inguinal scWAT**

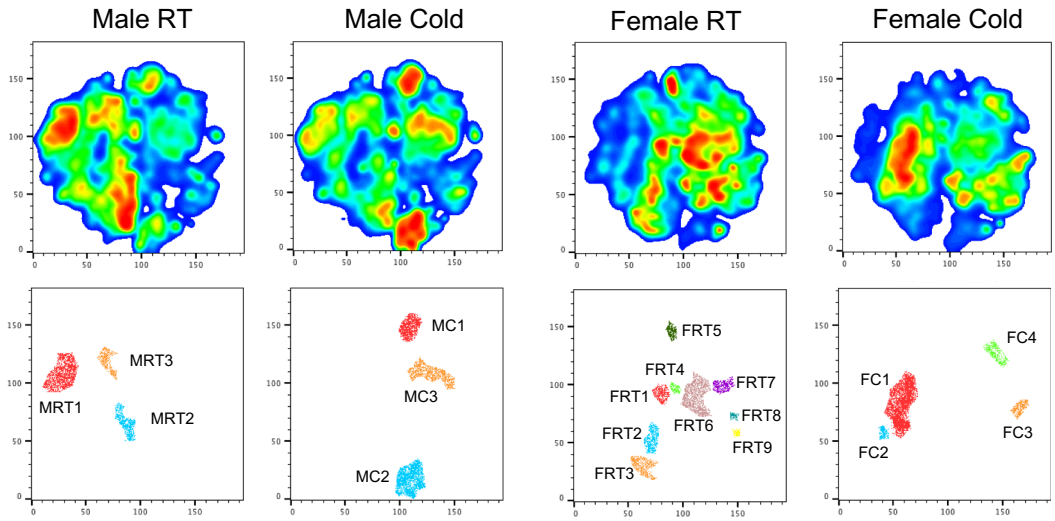

Population	%	Predicted Identity	Markers	
MRT1	9.2	Myeloid	CD11b⁺ CD62L⁺	Present in RT, Lost on Cold
MRT2	3.8	APC	CD11b^{neg}MHC⁺	Present in RT, Lost on Cold
MRT3	2.4	Myeloid	CD11b⁺CD62L^{neg}	Present in RT, Lost on Cold
MC1	5.6	T cells	CD11b^{neg} CD3⁺	Appear on cold
MC2	11.4	CINCs	CD11b⁺ CCR2⁺Cx3Cr1⁺	Appear on cold
MC3	5.8	T cells	CD11b^{neg} CD3+	Appear on cold
FRT1	2.4	B cells	CD11b^{neg} CD19⁺	Present in RT, Lost on Cold
FRT2	2.9	Monocyte	CD11b⁺ Ly6C⁺	Present in RT, Lost on Cold
FRT3	3.2	APC	CD11b^{neg}NK1.1⁺MHC⁺	Present in RT, Lost on Cold
FRT4	0.9	APC	CD11b^{neg} CD11c⁺	Present in RT, Lost on Cold
FRT5	1.8	APC	CD11b^{neg} CD62L⁺Ly6C⁺MHC^{mid}	Present in RT, Lost on Cold
FRT6	7.7	T cells	CD11b^{neg} CD3+	Present in RT, Lost on Cold
FRT7	2.1	T cells	CD11b^{neg} CD3+	Present in RT, Lost on Cold
FRT8	0.6	T cells	CD11b^{neg} CD3+	Present in RT, Lost on Cold
FRT9	0.6	APC	CD11b⁺ CD11c⁺	Present in RT, Lost on Cold
FC1	19.2	B cells	CD11b^{neg} CD19⁺	Appear on cold
FC2	1.1	B cells	CD11b^{neg} CD19⁺	Appear on cold
FC3	2.3	CINCs	CD11b⁺ CCR2⁺Cx3Cr1⁺	Appear on cold
FC4	2.5	T cells	CD11b^{neg} CD3⁺	Appear on cold

E. **Cold Induced CINCs**

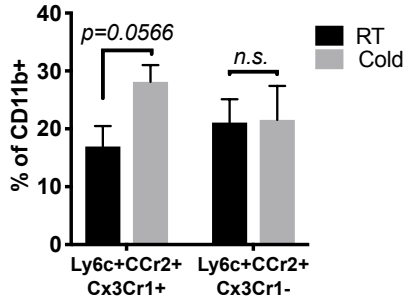
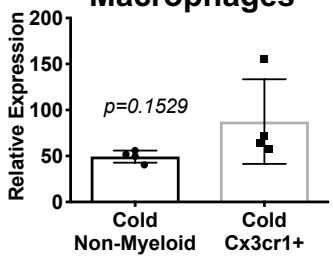
F. ***Bdnf* Gene Expression in CCR2+Cx3Cr1+ Macrophages**